Journal of Structural Geology, Vol. 5, No. 5, pp. 483 to 495, 1983
Printed in Great Britain

0191-8141/83 $3.00+0.00
Pergamon Press Ltd.

Displacement distribution along minor fault traces

HIROFUMI MURAOKA and HIROKI KAMATA

Geothermal Research Department, Geological Survey of Japan, Higashi 1-chome 1-3, Yatabe-machi, Tsukuba-gun, Ibaraki-ken 305, Japan

(*Received* 21 *December* 1982; *accepted in revised form* 12 *April* 1983)

Abstract—The variation of displacement along fifteen traces of minor normal faults was measured in the multilayered Quaternary sediments of Kyushu, Japan. In the diagrams of distance along a fault trace (L) vs displacement (D) two distinct types of faults, a cone-shaped L–D pattern (C-type) and mesa-shaped one (M-type), were detected. Because the L–D pattern is subject to slip-parallel strain in the wall rocks, a D-constant pattern is ascribed to the competent (rigid) material and a D-variable pattern is found in the incompetent material. Therefore, C-type faults are characteristic of homogeneous incompetent materials, whereas M-types are representative of faults that cut through a rigid unit. However, the steep slopes in the flanking sections of M-type patterns indicate that the faulting of a rigid unit should terminate in a strain absorber of incompetent materials. The concept of lithologic control in the L–D pattern is important for the better understanding of faulting processes as well as the localization of faults.

INTRODUCTION

BECAUSE faults are dislocations of rock units, geologists have long been analyzing fault movement through the recognition of fault displacement. It should be emphasized that displacement is commonly variable along and within a fault trace, and in any large fault displacement reduces towards the two ends of the trace. Therefore, the pattern of displacement distribution along a fault trace is critically important for understanding fault formation.

Chinnery (1963) pointed out that no measurement of the variation of displacement along a fault trace had been made by the early 1960s, but during the last two decades several active faults have been investigated (Brown & Wallace 1968, Matsuda 1972, 1974, 1976, Matsuda & Yamashina 1974, Tchalenko & Berberian 1975, Yamasaki *et al.* 1979). These workers presented distance along fault zone (L) vs displacement (D) or slip-rate (R) diagrams showing the multipolarized distribution of displacement along fault zones. Each fault displacement or slip-rate peak has generally been ascribed to segments of en échelon faults. These results have been supported by fault models including the heterogeneous dislocation or 'barrier model' that has been clarified from seismologic analyses of earthquake hypocenters (Das & Aki 1977, Aki 1979). The data on active faults are difficult to interpret because of the following factors. (1) The faults in most cases consist of so many fault traces that measured points of displacement are not available in sufficient quantity within a single fault segment. (2) Some faults have a complicated history of formation as a consequence of repeated movements. (3) The time–space complication makes it difficult to analyze the variation of displacement due to lithologic control.

We have been engaged in analyzing minor normal faults developed in Quaternary lacustrine sediments in the northern flanks of the Kuju volcano, Kyushu, Japan. In the course of the study, we often encountered completely exposed faults that exhibited both ends of the trace. Although they are small in size, the simplicity of the faults was an advantage from the viewpoint of analyzing displacement. (1) Much data were available within a simple fault segment. (2) Because they are paragenetic faults developed in the same rock units, their tectonic history is simple. (3) It is possible to analyze the displacement distribution related to lithological changes in the multilayered system.

This paper describes the displacement distribution along the minor fault traces, drawing attention to the existence of two distinct types of pattern, and discusses the geneses of the two with special reference to the nature of rock materials in the multilayered system. We also discuss the change of pattern due to the position of a fault trace on the fault plane.

OUTLINE OF GEOLOGY

The Kusu Group

Figure 1 shows the localities within the area investigated. The Kusu Group is sporadically exposed among the Quaternary volcanic rocks. The Kusu Group was previously regarded as late Miocene or Pliocene in age, but K–Ar dates obtained recently on the intercalated silicic lava indicate that the group is younger than 1 Ma; that is it is of Pleistocene age (Kamata & Muraoka 1982). The Kusu Group consists mainly of alternating lacustrine sediments such as diatomaceous siltstone, sandstone, mudstone and conglomerate intercalated with silicic lavas and tuffs. The lower contact of the group is not exposed, but from the exposed parts its maximum thickness is estimated to be about 400 m. It is divided into upper and lower formations by an intercalation of about 20 m of Nakamura pumice-flow deposits in

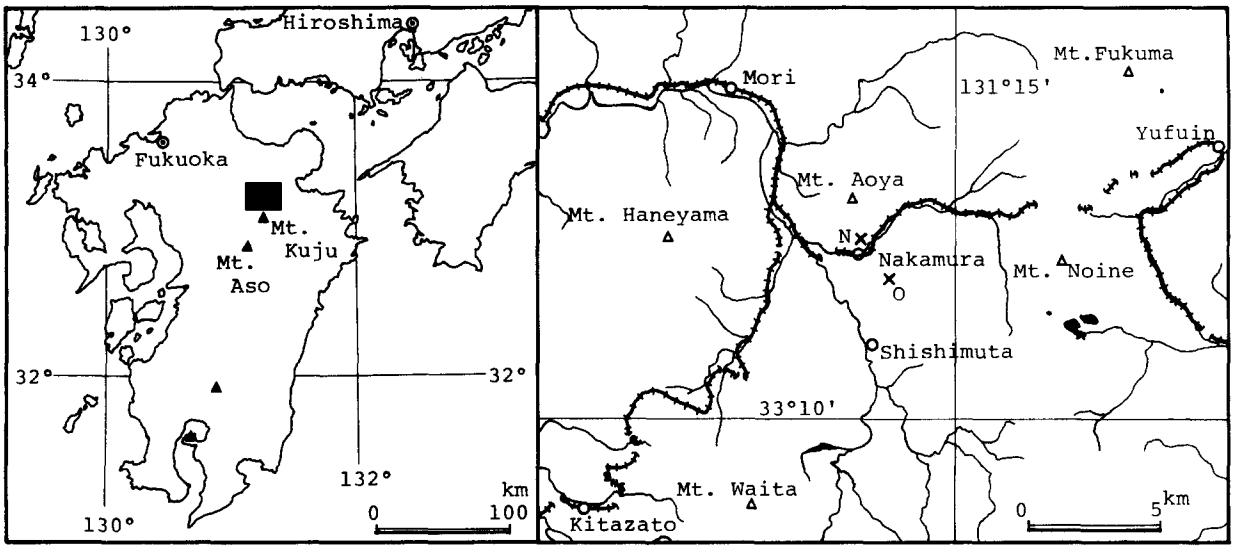

Fig. 1. Locality map. Crosses, N (Nakamura) and O (Okunameshi), show the quarries used as sampling localities. Hatched lines show railway tracks.

the middle horizon (Matsumoto *et al.* 1973). The bedding planes in the group are mainly horizontal or dip at less than 20°, but a number of N–S trending, partly overturned, folds have been reported from the Shishimuta area (Muraoka *et al.* 1980). These folds disappear northwards.

Localities N and O depicted in Fig. 1 are diatomite quarries where the upper formation of the Kusu Group crops out. In both quarries the strata are nearly horizontal and thin laminae are well developed.

Normal fault system

The main features of the E–W trending, minor normal faults have been reported already by Muraoka *et al.* (1981, in prep.) and their results are summarized here. Faults are densely developed in the so-called Hohi geothermal region; the rectangular-like graben 70 km (E–W) by 40 km (N–S). The fault system originated from N–S extension related to Quaternary volcanic activity in the region. Fault trends are locally parallel to lineaments visible on aerial photographs and Landsat images. This suggests that the minor faults have a paragenetic relationship to the large-scale faults visible as lineaments. The average displacement (vertical separation) on the minor faults is 8.8 cm and the average spacing is 1.6 m in a N–S direction. Figure 2 is a plot of poles to the minor fault planes. Although the cluster includes local changes of direction, the presence of conjugate sets is clearly indicated by the bipolar distribution of faults displaying N- and S-side downthrow directions. The average conjugate shear angle is 39°, rather small and possibly reflecting brittle behavior. Figure 3 shows the frequency distribution of vertical separations; each square representing the displacement of each fault

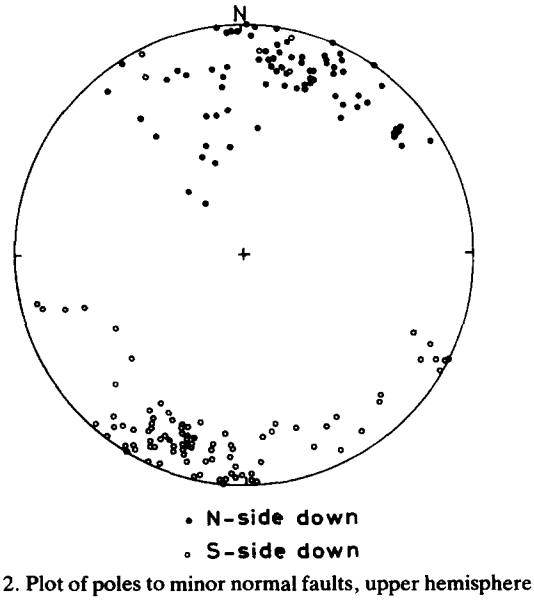

Fig. 2. Plot of poles to minor normal faults, upper hemisphere.

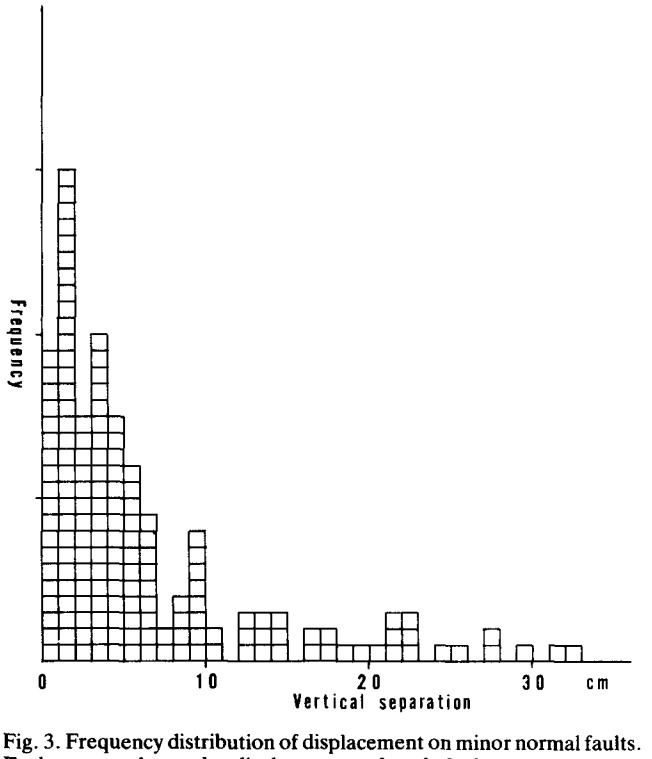

Fig. 3. Frequency distribution of displacement on minor normal faults. Each square shows the displacement of each fault measured at an arbitrary site along the trace.

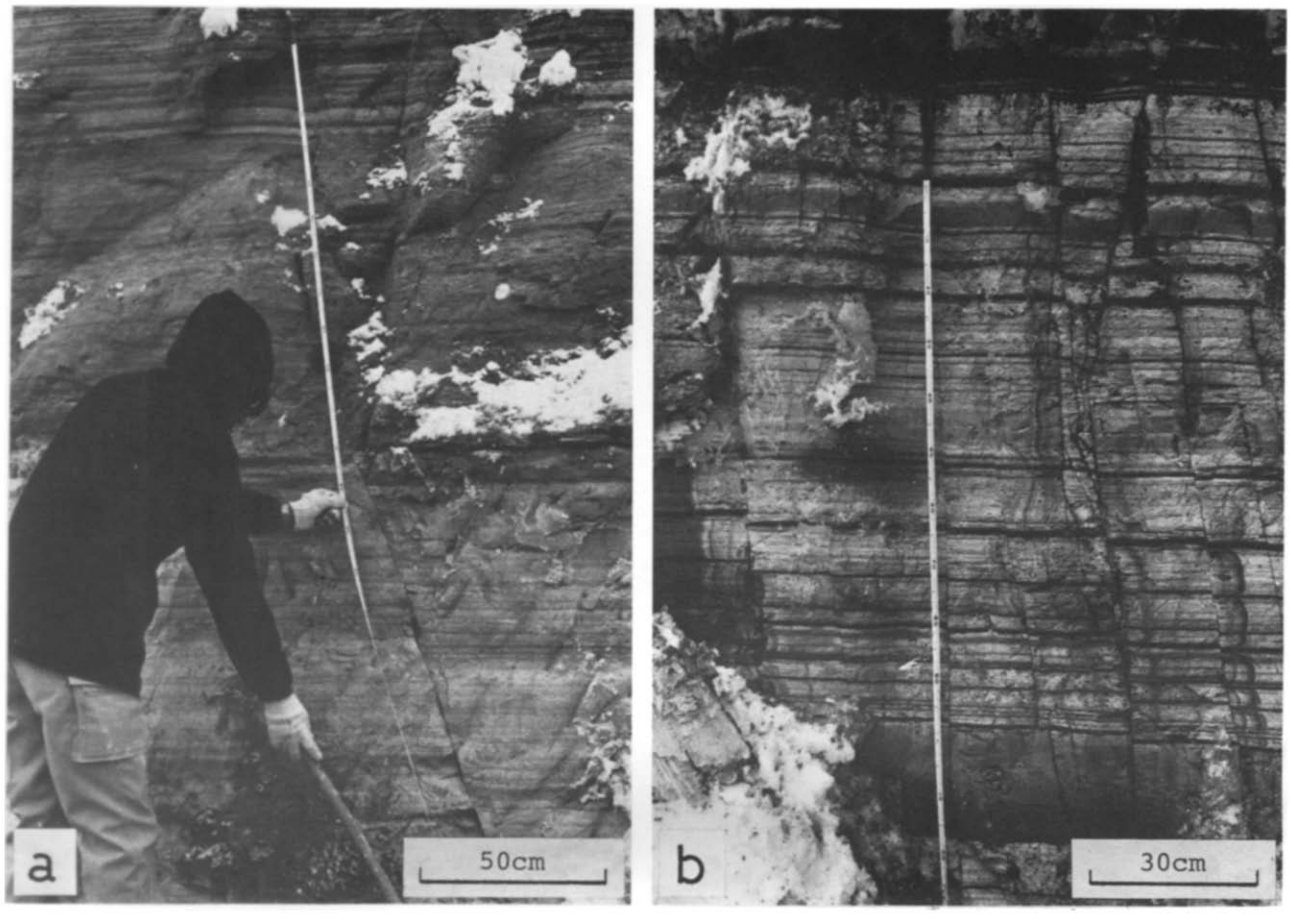

Fig. 4. (a) Fault No. 15. The displacement abruptly decreases upwards from the middle horizon within a soft sandstone.
(b) Fault No. 5. The displacement is small compared with the fault length.

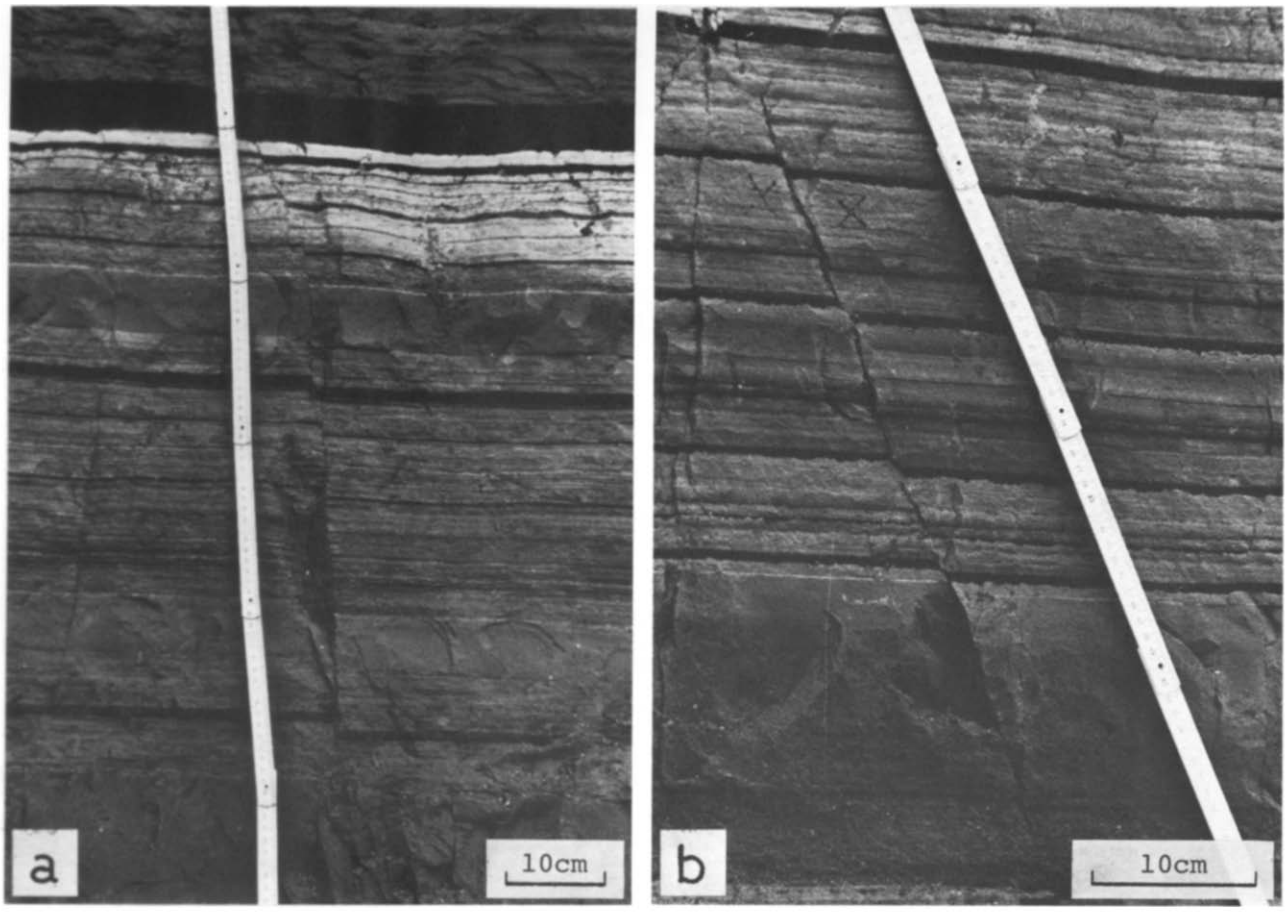

Fig. 9. Slip–parallel strain (layer-thickness strain) along faults Nos. 9 (a) and 10 (b). The layer-thickness between the two walls is nearly the same along these fault traces but is different near the ends of the traces.

measured at an arbitrary site along the trace. The pattern is similar to the shape for an exponential function, as has been pointed out elsewhere (Kakimi & Kodama 1974, Kakimi 1980). The fault system is thought to have been formed during a period of time ranging from the accumulation of the Kusu Group (younger than 1 Ma) to the Shishimuta folding phase (older than 0.3 Ma) according to Muraoka *et al.* (1981).

MEASUREMENTS

Fifteen minor faults were measured on the surfaces of vertical, N–S trending cliffs which are roughly perpendicular to the inferred σ_2-axis of the fault system. Most measurements were carried out on completely exposed faults that exhibited both ends of the fault trace. However, displacements on such short faults are generally too small to be measured by the naked eye, and for this reason we also measured half-exposed faults that displayed not only one end of the trace but also an apparent center of the trace as defined by the maximum displacement.

For each measurement, a tape-measure was laid parallel to and along the fault trace (Fig. 4). The position of each bedding- or lamination plane was determined in terms of the distance from one end along the trace, and the displacement was measured with this bedding- or lamination plane as a reference. Measurements were made from one end to the other end of the fault, each time noting any lithologic changes. Though position and displacement in most cases were measured to within 0.5 mm, the actual accuracy is considered to be in the order of millimeters. Because the position of displacement should be defined at the middle of a displaced bed, the data on one side of a wall were corrected where either addition or subtraction of half of the displacement value was carried out.

Measured displacement is not the vertical separation but the dip separation. Based upon the stress field suggested by the fault system, the strike separation is commonly negligible. In this case the net slip is better approximated by the dip separation rather than by the vertical separation, and therefore dip separation is used here as displacement.

DISPLACEMENT DISTRIBUTION

Table 1 gives the values of displacement, D, and the distance from one end along the trace, L, for 15 minor faults, illustrated as L–D diagrams in Figs. 5 and 6, within which different scales are used although the ratio between L- and D-axes is constant (1:25) throughout the 15 diagrams.

Two distinct types of L–D *patterns*

From Figs. 5 and 6, two distinct types of L–D patterns are recognizable. One type seems to be a triangle(cone)-shape such as displayed by faults Nos. 4–8 (Fig. 5b), while the other is a trapezoid(mesa)-shape such as shown

Table 1. Measurements of distance from one end along a fault trace, L, and displacement, D, for 15 minor faults.
Up, upper end of fault; Dn, lower end of fault

	No.1		No.2		No.3		No.4		No.5		No.6		No.7		No.8	
	Lcm	Dmm	Lcm	Dmm	Lcm	Dmm	Lcm	Dmm	Lcm	Dmm	Lcm	Dmm	Lcm	Dmm	Lcm	Dmm
	Up		Up		Up		Up		Up		Dn		Dn		Up	
1	0	0	0	0	0	0	0	0	0	0	0	0	0	0	0	0
2	2.1	2.0	1.8	1.5	2.0	0.5	1.2	0.3	0.9	0.5	2.9	1.0	1.8	0.5	1.0	1.0
3	3.6	2.5	3.2	3.0	2.7	0.5	1.4	0.5	1.9	0.5	3.9	1.5	3.5	1.0	5.4	1.0
4	6.8	3.0	4.4	6.0	4.4	1.0	3.1	0.7	2.7	1.0	9.1	2.5	5.3	1.5	10.9	1.0
5	10.9	3.0	5.2	6.5	4.8	1.0	5.8	1.0	4.0	1.5	10.1	4.0	8.8	2.0	18.2	3.0
6	13.1	3.5	6.3	8.5	12.5	1.5	7.0	1.5	5.4	1.5	10.8	4.0	10.8	2.5	28.8	5.0
7	13.8	3.5	7.3	8.5	13.3	1.5	8.0	1.5	7.3	1.5	16.1	4.5	11.8	3.0	30.5	6.0
8	14.7	3.0	8.4	9.0	13.6	1.5	11.1	2.0	7.6	1.5	21.0	5.0	13.6	3.0	32.1	6.5
9	19.8	3.0	10.6	10.0	16.1	1.5	11.6	2.0	8.8	2.0	25.3	5.0	20.2	4.0	39.5	10.0
10	23.2	3.5	12.5	9.5	17.0	1.5	13.1	2.0	10.1	2.0	28.4	6.0	27.3	5.0	42.3	11.0
11	24.8	4.0	15.7	8.0	19.7	2.0	15.4	2.0	12.0	2.0	31.7	6.5	35.8	6.0	47.4	13.0
12	28.5	4.0	17.0	8.5	25.8	3.0	17.1	2.5	13.4	2.0	33.6	7.0	44.6	8.5	55.3	13.0
13	33.4	3.5	18.4	8.0	26.7	3.0	18.9	3.0	14.8	2.0	38.1	7.0	46.4	7.0	57.5	13.5
14	34.5	3.5	19.5	6.0	29.7	3.0	24.9	3.0	18.5	2.5	40.7	7.0	50.2	8.0	65.1	13.0
15	36.5	3.0	20.9	6.0	42.7	3.0	30.2	3.5	19.5	2.5	50.9	7.5	52.3	9.5	69.3	13.0
16	38.8	3.0	24.0	5.5	44.0	3.0	31.7	3.5	21.9	3.0	60.2	5.5	59.6	11.0	74.7	10.0
17	42.2	3.0	26.5	2.5	50.5	3.0	32.1	3.5	22.9	3.0	65.7	5.5	61.8	12.0	81.8	6.0
18	43.5	2.5	28.1	2.5	52.2	3.0	34.0	3.0	26.2	3.0	69.7	5.0	63.1	12.0	82.6	6.0
19	49.7	2.0	30.4	3.0	54.2	3.0	42.0	2.5	30.9	4.0	70.9	5.0	68.1	12.0	84.7	5.0
20	51.2	1.5	32.3	1.5	57.0	3.5	43.0	2.5	32.6	4.5	72.8	4.5	72.3	13.0	87.4	5.0
21	54.6	1.0	34.0	0	57.5	3.5	44.3	2.5	34.3	4.5	78.8	3.0	74.2	13.0	93.7	5.0
22	56.0	1.0			61.8	3.5	48.6	2.0	36.3	5.5	80.9	2.5	78.7	13.0	96.8	4.0
23	57.3	0.5			68.5	19.0	49.9	2.0	42.8	6.0	85.4	2.0	82.5	13.0	104.9	4.0
24	58.7	0.5			69.1	18.0	52.1	1.7	45.4	7.0	88.9	2.0	89.6	14.0	111.8	3.0
25	61.2	1.0			70.0	18.0	52.5	1.7	51.7	7.0	91.4	1.0	93.0	14.0	112.7	2.5
26	63.3	1.0			71.9	18.0	53.7	1.5	54.1	7.5	95.9	1.0	96.3	16.0	119.1	1.5
27	69.0	0.5			76.8	17.0	55.8	1.0	58.5	7.0	98.7	0.5	97.9	17.0	122.3	1.0
28	73.2	0			79.6	15.0	57.1	1.0	61.1	8.0	103.0	0	107.4	18.0	128.3	0
29					86.2	15.0	58.7	1.0	62.6	8.0			112.4	19.0		
30					88.5	15.0	59.0	1.0	65.3	8.5			117.6	22.0		
31					89.5	15.0	61.2	0	67.1	8.5			122.7	23.0		
32					90.8	16.0			69.4	9.0			127.3	25.0		
33					95.7	14.0			72.3	8.5			131.3	26.0		
34					99.4	13.0			75.7	8.0			136.8	25.0		
35					102.6	11.0			76.4	8.0			142.4	27.0		
36					104.2	7.0			77.4	8.0			155.6	30.0		
37					106.2	13.0			79.2	8.0			175.1	34.0		
38									80.0	7.5			192.0	40.0		
39									92.2	7.5			216.0	32.0		
40									98.3	6.0			222.7	33.0		
41									102.2	5.5			229.5	30.0		
42									105.8	5.0			234.4	28.0		
43									110.5	4.5			239.4	27.0		
44									118.4	4.0			246.9	27.0		
45									123.7	3.5						
46									130.2	3.0						
47									139.1	2.5						
48									146.0	1.5						

	No.9		No.10		No.11		No.12		No.13		No.14		No.14'		No.15	
	Lcm	Dmm	Lcm	Dmm	Lcm	Dmm	Lcm	Dmm	Lcm	Dmm	Lcm	Dmm	Lcm	Dmm	Lcm	Dmm
	Up		Up		Up		Up		Dn		Up		Up		Up	
1	0	0	0	0	0	0	0	0	0	0	0	0			0	0
2	0.9	0.5	1.5	0.5	0.9	1.5	2.2	1.0	6.6	1.5	3.9	1.0			0.9	1.0
3	1.3	1.0	2.6	1.0	2.7	2.0	4.1	3.5	9.3	2.0	6.8	2.5			3.1	1.5
4	2.1	8.0	3.3	2.0	4.4	2.5	4.7	4.0	13.6	2.0	9.0	3.0			4.3	2.5
5	3.8	8.5	3.7	2.5	5.0	3.0	5.7	4.0	19.9	7.0	11.2	5.0			5.6	3.0
6	5.3	9.0	4.5	6.0	6.5	5.0	7.3	6.0	20.8	7.0	13.7	6.5			6.9	3.0
7	11.4	10.0	5.2	8.0	10.6	5.5	10.5	6.5	23.6	11.0	15.6	7.0			7.4	3.0
8	12.5	10.0	7.3	9.0	18.3	5.5	11.8	6.0	26.5	12.0	17.9	9.0			8.1	3.5
9	14.0	10.0	7.8	9.0	23.3	4.5	13.6	7.0	32.9	12.0	20.1	8.5			10.5	3.5
10	15.2	10.0	11.2	9.5	24.2	5.5	14.5	7.0	34.9	13.0	20.9	9.0			14.3	4.0
11	16.6	10.0	11.8	10.0	24.9	5.5	15.5	7.5	39.7	13.0	23.5	9.0			16.8	4.0
12	20.0	11.5	14.0	10.0	29.1	6.0	16.1	7.0	42.4	13.0	31.0	10.5			19.0	4.0
13	23.2	11.5	15.0	9.5	35.3	7.5	22.4	7.5	47.6	14.0	36.4	12.0			21.3	4.0
14	23.8	12.0	16.9	10.0	35.7	7.5	25.6	7.5	54.1	14.0	41.9	12.0			29.9	5.0
15	24.9	12.0	17.6	10.0	36.6	7.5	29.1	7.5	65.2	15.0	49.9	13.0			40.1	5.5
16	28.5	12.0	19.5	10.0	42.2	8.0	29.7	8.0	68.2	14.0	55.3	14.0			44.9	7.0
17	29.7	12.0	21.4	9.0	44.5	7.0	30.4	7.0	70.8	14.0	61.4	14.0			48.8	8.0
18	33.2	12.0	23.1	9.0	50.4	8.5	31.8	7.0	73.5	12.0	67.6	16.0			54.3	9.0
19	35.4	13.0	23.9	9.0	53.0	8.0	32.8	6.5	79.4	13.0	67.9	16.5			57.7	10.0
20	37.6	13.0	27.1	8.5	59.0	7.0	45.0	0	85.5	13.0	70.1	17.0			62.0	15.0
21	42.8	16.0	27.6	8.5	61.4	7.0			91.5	12.0	75.1	18.0			76.0	20.0
22	45.8	15.0	29.7	8.0	62.0	6.0			108.3	12.0	78.6	17.0			88.6	20.0
23	47.8	15.0	31.4	8.0	65.3	5.5			112.1	11.0	79.6	18.0			97.2	24.0
24	48.5	14.5	31.8	8.0	66.0	5.5			118.9	12.0	92.3	16.0			108.1	48.0
25	53.6	12.0	32.7	8.0	67.1	5.0					97.9	15.0			118.2	61.0
26			33.4	7.5	68.6	3.5					102.4	13.5			122.0	61.0
27			34.1	8.0	81.0	0					112.3	14.0			136.1	70.0
28			34.7	8.0							114.3	14.0			142.3	70.0
29			35.7	8.0							117.8	14.0			148.0	70.0
30			49.2	6.5							128.6	13.5	133.0	0	156.2	73.0
31			54.7	5.5							133.9	8.0	134.4	8.0	157.2	73.0
32			55.5	5.0							137.9	1.5	138.4	19.0	161.2	76.0
33			57.1	3.0							142.9	1.0	140.2	15.5	172.7	77.0
34			57.8	2.5							145.0	0	142.2	15.5	192.3	78.0
35			60.3	1.0									143.2	16.0	204.4	80.0
36			61.0	0									146.9	15.0	205.5	80.0
37													149.0	15.0	217.0	83.0
38													153.2	11.0	223.3	86.0
39													156.4	11.0	232.0	80.0
40													157.5	10.0	240.6	77.0
41													162.3	13.0	251.3	73.0
42													171.0	20.0	255.3	78.0
43															267.2	74.0

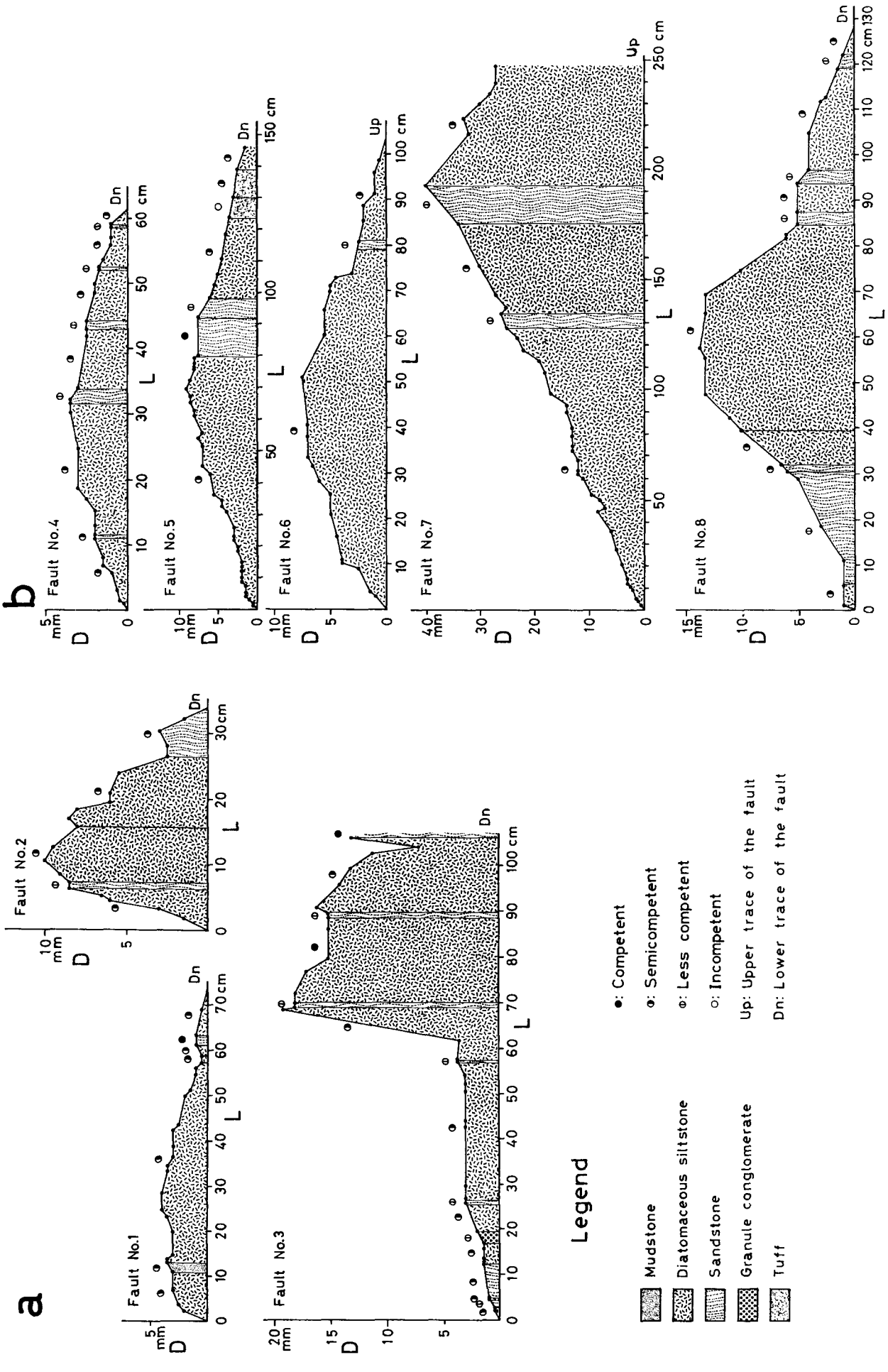

Fig. 5. (a) *L–D* diagrams of undivided type faults. *L*, distance from one end along a fault trace; *D*, displacement in the direction of dip separation. (b) *L–D* diagrams of C-type faults. Legend as in (a).

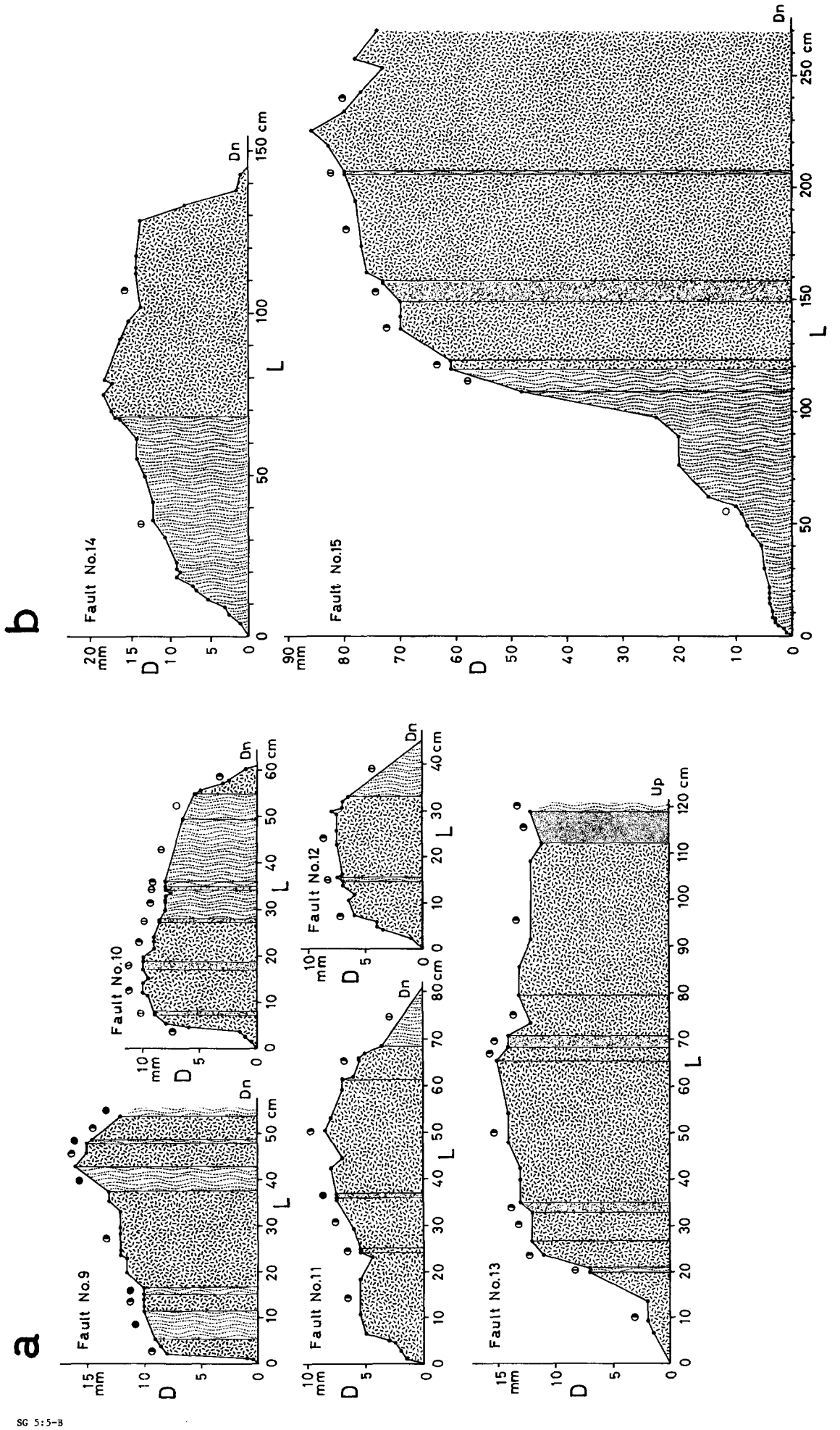

Fig. 6. (a) & (b) *L–D* diagrams of M-type faults. See Fig. 5 for legend and explanation of symbols.

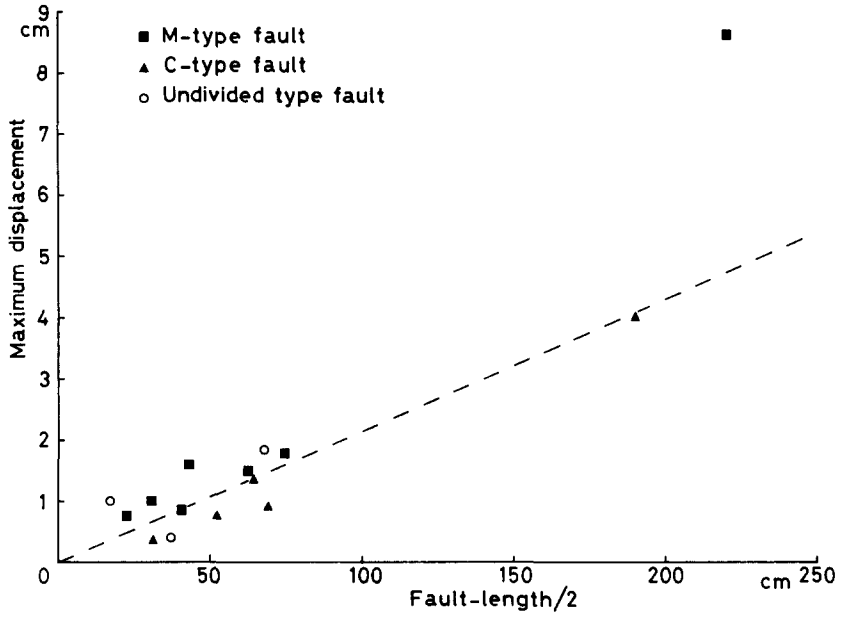

Fig. 7. Relationship between fault half-length and maximum displacement. Broken line shows the discriminative line ($D_{max} = 3/280L_t$) separating the fields of C- and M-type faults.

by faults Nos. 9–15 (Figs. 6a & b). We call the former C-types and the latter M-types. The other three faults, Nos. 1–3, show somewhat complicated *L–D* patterns and they are difficult to classify into either category (Fig. 5a). The C-type is characterized by a nearly symmetrical shape with a gentle change of displacement. The *L-D* curves are considered to be linear as a first approximation. The M-type consists of a broad, central section with no significant change of slope and flanking portions with an abrupt change of displacement shown by the steep slopes of the graphs. The flanking curves tend to be concave upwards.

C- and M-types are also distinguished quantitatively by another criterion. Figure 7 shows the relationship between the fault length, L_t, and the maximum displacement, D_{max}, where the former is given in terms of $L_t/2$ because the parameter for the half-exposed faults can only be estimated as the length from one end ($D = 0$) to the apparent center (D = max). Positive correlations in Fig. 7 are not high as a whole. However, each cluster of C- and M-types shows a better correlation. It should be noted that the fields of the two types are clearly divided by the discriminative line ($D_{max} = 3/280L_t$), and that the D_{max}/L_t ratio of the M-type is nearly twice as large as that of the C-type. This means, if the faults are of the same length, that the average displacement $\bar{D}$ along the fault trace of an M-type is much larger than twice that of a C-type, due to the shape of the patterns. Based upon this criterion, fault No. 1 may be close to a C-type and Nos. 2 and 3 may be those of an M-type.

Lithologic control on L–D *patterns*

Wall rocks contain thin layers as seen in the spacing of the measured points of D in Figs. 5 and 6. The most dominant layers are of diatomaceous siltstone, which is fairly hard and compact. Sandstone and tuff layers are commonly soft and loosely compacted, but their fine-grained parts are occasionally harder than siltstone layers. We attempted to qualitatively classify the relative hardness or competency into four classes for the outcrops illustrated in Figs. 5 and 6. The shear angle between conjugate faults is known to reflect ductility or competency of rock units. Shear angles observed in the Kusu Group are clearly different between siltstone (17–45°) and sandstone (45–69°). It may be that in the Kusu Group siltstones are generally more brittle and competent than sandstones.

L–D patterns seem to be controlled directly by the characters of each of the layers. Most of the *L–D* diagrams contain rather irregular curves and thus it is difficult to discuss the variations of slopes from layer to layer. However, it is possible to compare curves between the thick siltstone layers and the thick sandstone layers. For instance, a sloping shoulder in the lower trace of fault No. 10 (the right half of the *L–D* pattern) seems to be derived from the thick, less competent sandstone layers. Likewise, a sloping shoulder in the upper trace of fault No. 14 (the left half of the *L–D* pattern) seems to be connected with the thick, less competent sandstone layers. A most important example is shown by fault No. 15, whose wall rocks are composed chiefly of two contrasting lithologic units; semicompetent siltstone and incompetent sandstone (see Figs. 4a and 6b). The displacement is constantly large in the siltstone (the right half of the *L–D* pattern) but abruptly decreases in the sandstone (the left half of the *L–D* pattern). The incompetent sandstone seems to be responsible for the abrupt decrease of D in the upper trace of this fault. Although there remains the ambiguity of competency estimation within the dominant siltstone layers, it seems that the competent layers show D-constancy and the incompetent layers show D-variability.

Interference effect of neighboring faults on L–D *patterns*

En échelon faults were often recognized in the dense network of fractures exposed in the cliffs. Neighboring segments of en échelon faults should interact with each other in *L–D* patterns. Although most of the fault traces discussed here are rather isolated, fault No. 14 is associated with a neighboring fault (Fig. 8a). The interaction between the two *L–D* patterns is illustrated in Fig. 8(b). It indicates a reciprocal relationship, where the decrease of *D* in one segment is marked by an increase of *D* in another. As a result the overall *L–D* pattern is not so discontinuous (Fig. 8b).

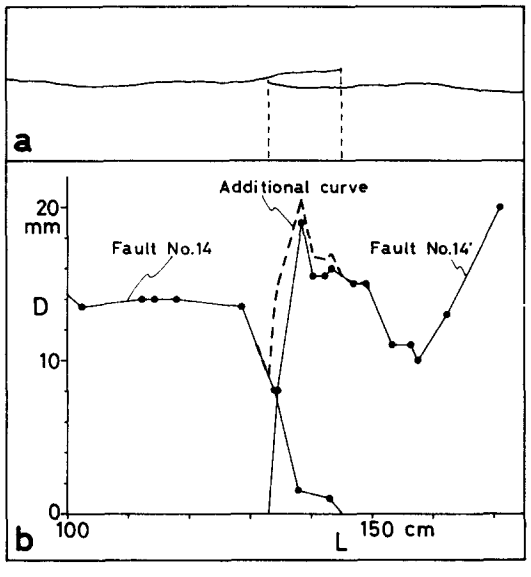

Fig. 8. Interaction of *L–D* patterns between neighboring faults. (a) Shape of the fault traces. (b) *L–D* patterns.

DISCUSSION

Geneses of two types of L–D *patterns*

Let us consider how displacement changes along a fault trace. If the displacement was constant along the trace, the fault should be endless due to perfect parallel movement of both sides of the walls. In other words, a change of displacement is impossible without variation in 'the slip–parallel strain' which is the strain of the wall rocks in the direction of net slip (Fig. 9). Because the studied faults are nearly orthogonal to the layers, the slip–parallel strain can be referred to here as the layer-thickness strain. Figures 10(a) & (b) represent the idealized *L–D* patterns of C- and M-type faults, respectively. These geometrical patterns are attributed to the two types of changes in the layer-thickness strain illustrated in Figs. 10(c) & (d), where all the layers are assumed to have been of the same thickness with the exception of the rigid unit. It should be emphasized that the slope of the curves in *L–D* diagrams is directly proportional to layer-thickness strain, irrespective of whether the strain was contractional or extensional. The *L–D* patterns can, therefore, be used as indicators of the nature of behavior of the rock materials.

For instance, the slopes of C-type curves which are generally constant indicate uniform distribution of layer-thickness strain along the fault trace (Figs. 10a & c). Whereas, the negligible slope of the broad central sections of M-type faults indicates parallel movement with no significant change in the layer-thickness strain. This feature is typical of rigid units acting as competent layers (Figs. 10b & d). Therefore, C-type faults are characteristic of incompetent layers and M-type faults are those which cut through rigid units or competent layers. However, one important observation is that M-type patterns

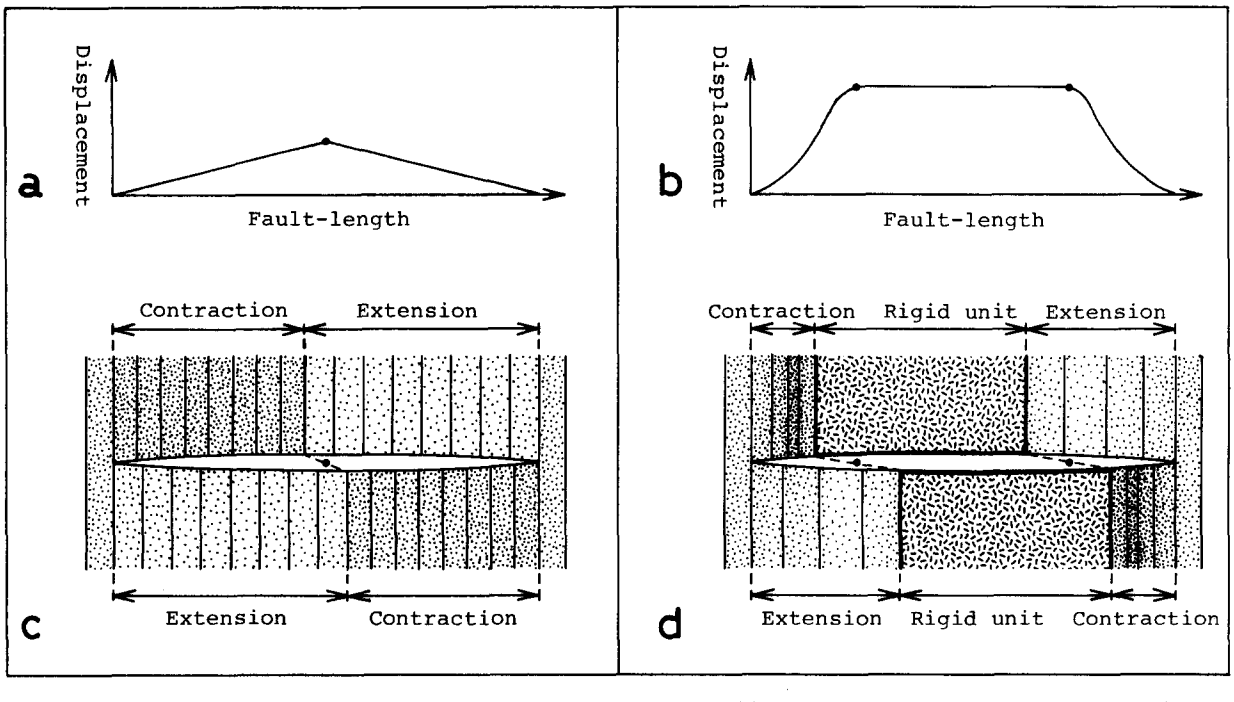

Fig. 10. Models showing derivations of C- and M-type *L–D* patterns. (a) Idealized *L–D* pattern of a C-type fault. (b) Idealized *L–D* pattern of an M-type fault. (c) Idealized strain of a C-type fault. (d) Idealized strain of an M-type fault.

usually display a steep slope in the flanking sections of the curve. This clearly indicates that faulting of rigid units usually terminates in the sandwiching incompetent layers. A rigid unit itself tends to exclude the strain change as well as the displacement change. From the viewpoint of faulting processes, we propose that a rigid unit can be displaced whenever a fracture entirely cuts that unit and enters the incompetent layers. Even though the flanking sections of M-type patterns are present in the incompetent layers, their curves tend to be concave upwards and the slope is much steeper than that of C-type patterns. These observations may be attributed to a constraint by the active behavior of competent layers in M-type faults, while the incompetent layers act as passive strain absorbers. The concept of competency between active competent layers and passive incompetent layers is similar to that employed to visualize the folding of a multilayered system. The above interpretations are consistent with the observation that the hard layers show D-constancy and soft layers show D-variability in graphs.

Another important observation is that the average displacement $\bar{D}$ of M-type faults is more than twice that of C-type faults for the same fault-length. The stress drop $\Delta\sigma$ associated with faulting can be estimated by the equation $\Delta\sigma = c\mu\bar{D}/L_t$, where c is a constant defined by both the shape of the fault plane and the slip-direction of the fault and μ is the modulus of rigidity. The equation suggests that the stress drop, $\Delta\sigma$, of M-type faults is more than twice that of C-type faults. This is in broad agreement with the competency difference of the layers mentioned above. It indicates that a rigid unit composed of competent layers acts as a sharp stress concentrator in the M-type faulting process, because the fracture of competent materials with low ductility requires a large ultimate stress as well as a large stress drop (Mogi 1972). Competent layers may play a role as either initiators or inhibitors of faulting, depending on whether the stress concentration exceeds the ultimate stress, or not. The role of competent layers may be comparable to that of a brittle barrier during earthquake rupturing as has been suggested from a seismologic viewpoint by Aki (1979).

Profile effect on L–D *patterns*

An important factor is that displacement is distributed over a fault plane, though it is difficult to observe. Let us assume a fault plane to be circular and the patterns of displacement distribution on the fault plane to be axially symmetrical. If these assumptions are reasonable, the L–D patterns should be controlled by the position of a section through the fault plane. We call this the 'profile effect'. It is to be expected that with the profile effect the nearer the trace approaches to the center on the fault plane, the greater the D_{max}/L_t ratio varies with the change of L–D patterns.

M-type faults are not suitable for examination of such a profile effect because of the constraint introduced by the heterogeneous lithology, but C-type faults may be used. Figure 11(a) shows the relationship between the D_{max}/L_t ratio and L–D patterns for five faults of C-type where the L value is normalized by the available L_t as 1.0, or the apparent $L_t/2$ as 0.5, and the ratio between L- and D-axes is retained as 1:100. Although in previous

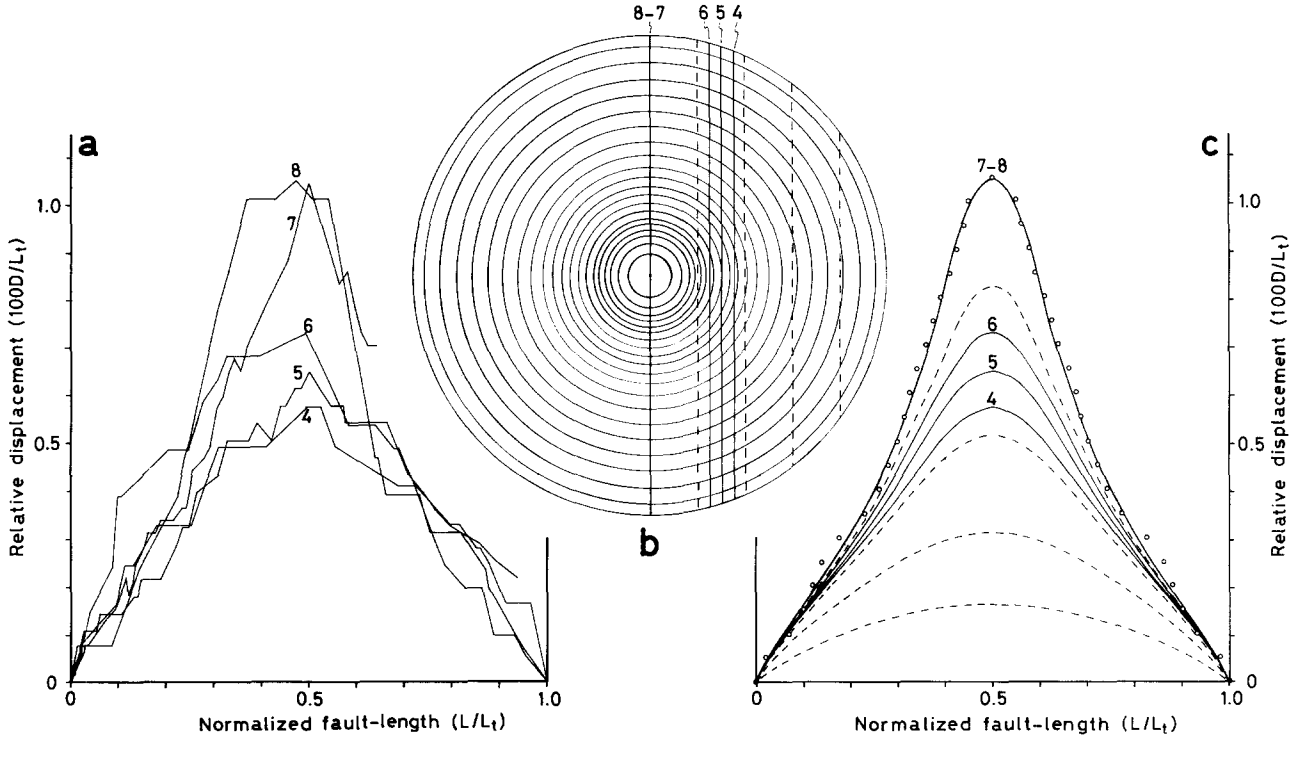

Fig. 11. Change of L–D patterns derived from the profile effect. (a) L–D patterns of C-type faults. (b) Tentative contour map showing the displacement distribution on a fault plane. The central profile is assumed to be the average of faults Nos. 7 and 8. Sites of faults Nos. 4 to 6 are determined by the D_{max}/L_t ratio. (c) Change of L–D patterns due to the position of the profiles on the contour map of (b). Open circles show the average of faults Nos. 7 and 8 simplified into a smooth curve.

sections both flanking curves of C-type patterns have been considered to be linear as a first approximation, it is clear from Fig. 11(a) that the curves are varying with change in the D_{max}/L_t ratio. That is to say, the curves of high D_{max}/L_t faults (e.g. Nos. 7 and 8) tend to be concave upwards while those of low D_{max}/L_t faults (e.g. Nos. 4–6) tend to be convex upwards. This relationship supports the existence of the profile effect. It also implies that faults Nos. 7 and 8 are representative of traces near the center on the fault plane, and the other three represent sections at some distance from the fault center. If we assume that faults Nos. 7 and 8 reveal the central profile of displacement distribution on a fault plane, we may produce a contour map of the displacement distribution on the fault plane as shown in Fig. 11(b). The profile that is the *L–D* pattern averaged from faults Nos. 7 and 8 is shown in Fig. 11(c). In addition the localities equivalent to each D_{max}/L_t ratio of the other three faults are represented in Fig. 11(b), and their adapted *L–D* patterns are illustrated in Fig. 11(c).

The correlation between the actual patterns illustrated in Fig. 11(a) and schematic patterns shown in Fig. 11(c) is not good in detail. Nevertheless, it should be noted that the general change among *L–D* patterns, ranging from concave to convex upwards is consistent. It may be that the change of C-type patterns is controlled geometrically by the profile effect. This is thought to hold even if a fault plane is assumed to be ellipsoidal instead of circular. Thus we derive a criterion to know whether, or not, a given trace of a C-type fault is off center on a fault plane. It is not clear why the slopes shown in Fig. 11(b) should be concave upwards, but a possible explanation may be that the localization of a fault center takes place in a relatively hard portion even within apparently incompetent layers, because fault initiation requires a stress raiser.

Implication for faulting processes

The concept of lithologic control on *L–D* pattern is useful for understanding faulting processes. Figure 12 schematically illustrates a general arrangement of normal faults in rhythmically alternating competent and incompetent layers. A rigid unit responsible for the formation of short M-type faults is not necessarily effective for a long fault by the scaling law, and therefore long faults tend to be of C-type even if the rigid unit makes the *L–D* curve level over a small range. Furthermore, though the displacement distribution macroscopically continues over neighboring segments of en échelon faults, they should also be associated with layer-thickness strain at the sites of interchanges of fault traces. This suggests that such interchanges of en échelon faults tend to occur in incompetent layers owing to their roles as strain absorbers.

Figure 13(a) shows the aseismic slip (fault creep) rate along the Watsonville–Cholame segment of the San Andreas fault, measured during the period 1966–1979 from alignment array surveys by Burford & Harsh (1980). The San Andreas fault is one of the most intensively studied large-scale active faults. Although the diagram employs the slip-rate (*R*) instead of displacement, the pattern can be interpreted in a similar way to an *L–D* diagram, because the *L–R* pattern is comparable to an *L–D* pattern over a certain period. Using our terminology, the pattern appears to be of C-type as a whole, but it is likely that competent or rigid materials are present in the relatively flat portions of the *L–R* curve, such as the central section and two steps in the northwest part of the region. Figure 13(b) shows a generalized geologic map along the segment simplified from Jennings (1977). It is remarkable that the flats of the central section and the northwestern step are consistent with the distribution of crystalline rocks in contact with the fault trace (i.e. the metamorphic rocks of the Franciscan Group and the Mesozoic granitic rocks, respectively) among the dominant Tertiary sediments. It may be that these flat portions of the *L–R* curve are related to lithologic control exerted by competent materials during fault movement. However, one difficulty of this explanation is that the equivalents of the crystalline rocks cannot be found on the other side of the fault due to the large displacement.

We wish to emphasize that displacement distributions along faults are strongly controlled by differential strain in heterogeneous rock materials in the walls.

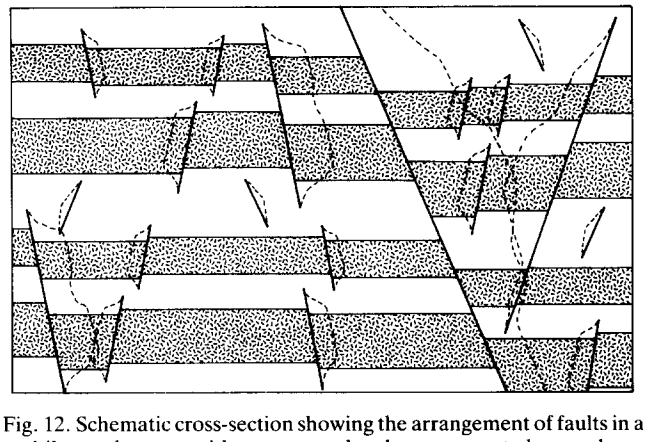

Fig. 12. Schematic cross-section showing the arrangement of faults in a multilayered system with ornamented and unornamented areas showing competent and incompetent layers, respectively. Broken lines represent the *L–D* patterns.

CONCLUSIONS

(1) Faults display two distinct types of *L–D* pattern. One is composed of symmetrical sections with a gentle change of *D* giving rise to cone-shaped (C-type) graphs. The other consists of a broad central section with no significant change of *D*, and flanking sections with an abrupt change of *D* to give mesa-shaped (M-type) graphs.

(2) The genetic contrasts between the two are recognized by the relationship between the fault length (L_t) and the maximum displacement (D_{max}); the D_{max}/L_t ratio of M-type faults being approximately twice that of C-type faults.

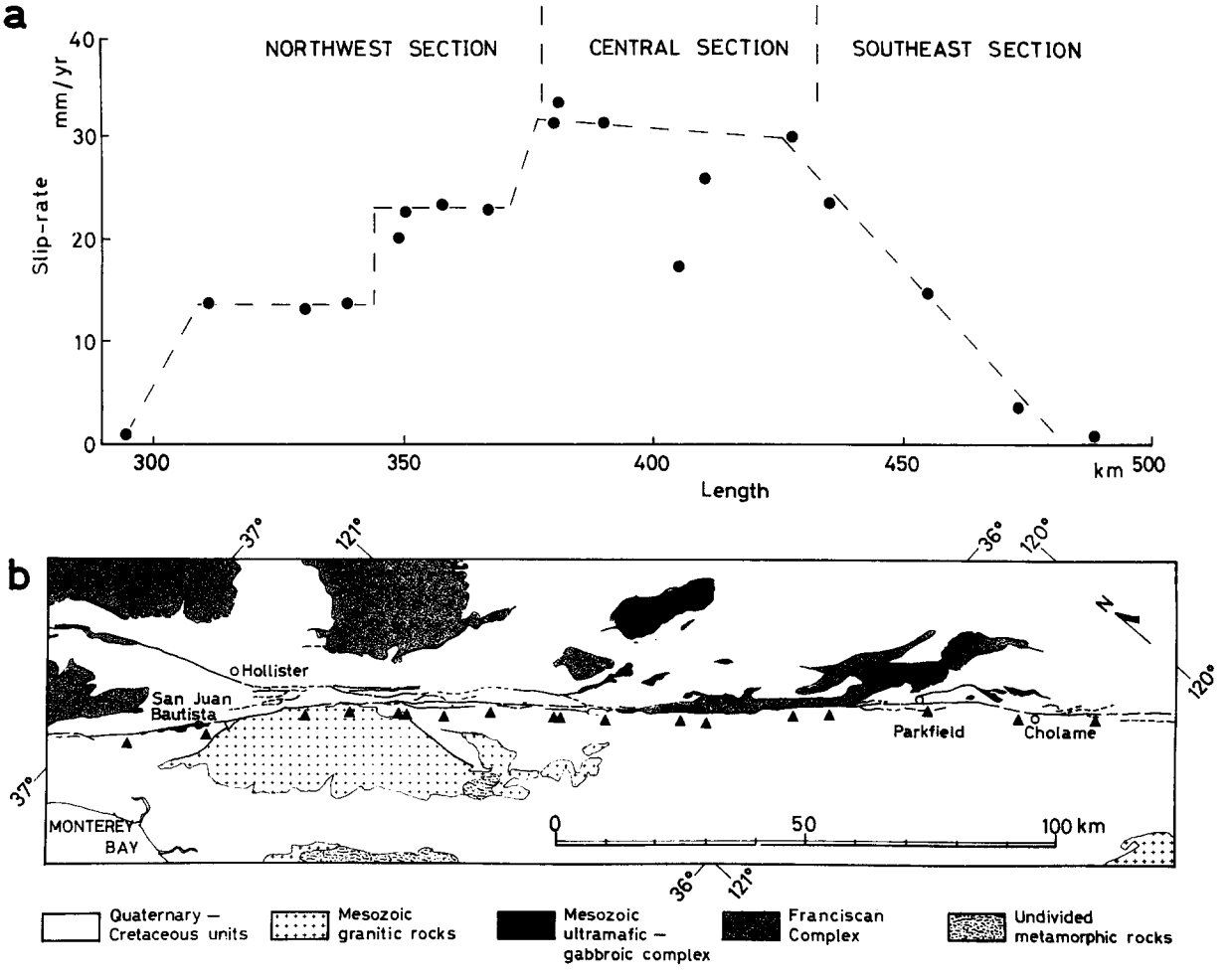

Fig. 13. (a) Aseismic slip rates along the Watsonville–Cholame segment of the San Andreas fault, measured during the period 1966–1979 from alignment array surveys (from Burford & Harsh 1980). Length is given in kilometers southeast of Point Arena, California. (b) Geologic map along the Watsonville–Cholame segment of the San Andreas fault (simplified from Jennings 1977). Closed triangles show measurement sites.

(3) The slope of L–D curves is directly proportional to the slip–parallel strain of the wall rocks (referred to here as the layer-thickness strain), and therefore the patterns can be used as indicators of the nature of behavior of rock materials.

(4) Because of their constant slope along the trace C-type faults are considered to be characteristic of soft and homogeneous incompetent layers.

(5) M-type faults are those which cut through a rigid unit or a competent layer and they display a flat central section to the curve. However, the steep slopes in the flanking sections indicate that the faulting of a rigid unit usually terminates in a strain absorber—an incompetent layer.

(6) The role as a stress concentrator of a rigid unit, inferred from the high D_{max}/L_t ratio of M-type faults, is probably consistent with the concept of a brittle barrier for earthquake ruptures as suggested by Aki (1979).

(7) The minor changes among C-type patterns seem to vary with the D_{max}/L_t ratio, and may be controlled geometrically by the position of the section through the fault plane (the profile effect).

Acknowledgements—We thank Mr. Y. Kinugasa and Dr. H. Hase of the Geological Survey of Japan for their valuable suggestions in the field and for their critical reading of the manuscript. Dr. T. Kakimi of the Geological Survey of Japan and Prof. T. Uemura of Niigata University also critically read the manuscript. This paper benefited from the comments of two anonymous referees.

REFERENCES

Aki, K. 1979. Characterization of barriers on an earthquake fault. *J. geophys. Res.* **84**, 6140–6148.

Brown, R. D. & Wallace, R. E. 1968. Current and historic fault movement along the San Andreas fault between Paicines and Camp Dix, California. In: *Proceedings of the Conference on Geologic Problems of San Andreas Fault System* (edited by Dickinson, W. R. & Grantz, A.). *Stanford University Publ. geol. Sci.* **11**, 22–39.

Burford, R. O. & Harsh, P. W. 1980. Slip on the San Andreas fault in central California from alinement array surveys. *Bull. seism. Soc. Am.* **70**, 1233–1261.

Chinnery, M. A. 1963. The stress changes that accompany strike-slip faulting. *Bull. seism. Soc. Am.* **53**, 921–932.

Das, S. & Aki, K. 1977. Fault plane with barriers: a versatile earthquake model. *J. geophys. Res.* **82**, 5658–5670.

Jennings, C. W. 1977. *Geologic Map of California, Scale* 1:750,000. State of Calif. and Calif. Div. of Mines and Geol.

Kakimi, T. 1980. Magnitude–frequency relation for displacement of minor faults and its significance in crustal deformation. *Bull. geol. Surv. Japan* **31**, 467–487.

Kakimi, T. & Kodama, K. 1974. Frequency distribution of faults in respect to throw, with special reference to crustal deformations and seismicities (preliminary note) (in Japanese, with English abstract). *Bull. geol. Surv. Japan* **25**, 75–87.

Kamata, H. & Muraoka, H. 1982. K-Ar ages of the volcanic rocks in the central part of Oita Prefecture, southwestern Japan (in Japanese, with English abstract). *Bull. geol. Surv. Japan* **33**, 561–567.

Matsuda, T. 1972. Surface faults associated with Kita-Izu earthquake of 1930 in Izu Peninsula, Japan (in Japanese, with English abstract). In: *Izu-Hanto* (edited by Hoshino, M. & Aoki, H.). Tokai University Press, Tokyo, 73–93.

Matsuda, T. 1974. Surface faults associated with Nobi (Mino–Owari) earthquake of 1891, Japan (in Japanese, with English abstract). *Spec. Bull. Earthquake Res. Inst. Tokyo Univ.* **13**, 85–126.

Matsuda, T. 1976. Active faults and earthquakes—the geological aspect (in Japanese, with English abstract). *Mem. geol. Soc. Japan* **12**, 15–32.

Matsuda, T. & Yamashina, K. 1974. Surface faults associated with the Izu-Hanto-oki earthquake of 1974, Japan (in Japanese, with English abstract). *Spec. Bull. Earthquake Res. Inst. Tokyo Univ.* **14**, 135–158.

Matsumoto, Y., Sakata, T., Matsuo, K., Hayashi, M. & Yamasaki, H. 1973. Volcanic geology of the northern foot of the Kuju volcano group, central Kyushu, Japan (in Japanese, with English abstract). *Kyushu Univ. Res. Inst. Ind. Sci. Rept.* **57**, 1–15.

Mogi, K. 1972. Fracture and flow of rocks. *Tectonophysics* **13**, 541–568.

Muraoka, H., Kamata, H. & Hase, H. 1980. Tectonic significance of the overturned fold found in the northern flanks of the Kuju volcano group (in Japanese, with English abstract). *Bull. geol. Surv. Japan* **31**, 599–608.

Muraoka, H., Kamata, H. & Hase, H. 1981. Geologic structure and minor faults in the northern flanks of the Kuju volcano group (in Japanese). *Abstr. geol. Soc. Japan*, 313.

Muraoka, H., Hase, H. & Kamata, H. in prep. Structure and tectonics of the so-called Hohi geothermal region, Kyushu, Japan.

Tchalenko, J. S. & Berberian, M. 1975. Dasht-e Bayas fault, Iran: earthquake and earlier related structures in bedrock. *Bull. geol. Soc. Am.* **86**, 703–709.

Yamasaki, H., Koide, H. & Tsukuda, E. 1979. Surface faults associated with the Izu–Oshima–Kinkai earthquake of 1978, Japan. *Spec. Rep. geol. Surv. Japan* **7**, 7–35.